Electrical Power and Energy Systems 141 (2022) 108140

Contents lists available at ScienceDirect

International Journal of Electrical Power and Energy Systems

journal homepage: www.elsevier.com/locate/ijepes

Power-flow-based energy management of hierarchically controlled islanded AC microgrids

Sarthak Chopra *, Gowtham Meda Vanaprasad, Gibran David Agundis Tinajero, Najmeh Bazmohammadi, Juan C. Vasquez, Josep M. Guerrero

Center for Research on Microgrids (CROM), AAU Energy, Aalborg university, 9220 Aalborg, Denmark

ARTICLE INFO

Keywords:
Energy management
Islanded AC microgrid
Hierarchical control
Power flow
Energy storage system

ABSTRACT

This paper presents a novel approach of employing hierarchical control to optimize the operation of islanded AC microgrids. The proposed method is an offline, centralized, power-flow-based energy management scheme which includes primary and secondary control dynamics in a modified power-flow formulation. The inner power-flow level maintains bus voltages and system frequency within the desired range and ensures power balance in the network. The outer optimization level ensures that the various components remain within their operational constraints, while optimizing a system-level objective. Two case studies are explored using a modified 14-bus medium voltage (MV) CIGRE benchmark microgrid to validate the proposed energy management algorithm. The first case includes minimization of conventional generator operating cost and renewable energy curtailment, both with linear and non-linear loads, and the second case includes minimization of conventional generator operating cost with load shedding. The results obtained from the case studies show the efficiency of the proposed energy management algorithm, and evidence its reliability for the optimal operation of islanded AC microgrids with multiple renewable energy sources.

1. Introduction

The extensive promotion of green energy and decarbonization, through the various environmental policies and initiatives, have driven research towards innovative solutions. In this regard, renewable energy sources (RES) and complementary technologies have received wide global attention. This has propelled a rise in decentralizing the power system through deploying distributed energy resources (DERs). Microgrids have emerged as an promising means of interconnecting DERs to the distribution grid [1]. Microgrids are formed by the accumulation of distributed generation (DG) units, energy storage systems (ESS) and loads that operate in conjunction with each other to ensure reliable power supply to the microgrid network [2]. Additionally, they can operate in grid-connected mode by being connected to the distribution grid through a point of common coupling (PCC), or independently of the distribution grid in islanded mode. Fig. 1 displays a schematic representation of a microgrid with conventional generators (CGs), RES such as wind turbines (WTs) and solar photovoltaic (SPV) panels, ESS, loads and the main utility grid, along with a centralized energy management system (EMS).

Microgrids offers various technical, economical, and environmental benefits [3]. They support remote area electrification, reduce power outages, and improve the energy efficiency in the system. Microgrids also reduce system losses and provide ancillary services to ensure economical operation. Environmental benefits may include the increased use of RES which help in minimizing emissions and carbon footprint. Microgrids are, however, associated with many challenges such as low inertia, system stability, power quality, power sharing among the DGs, maintaining voltage and frequency, and communication related challenges [2,4,5]. Naturally, a comprehensive control scheme is required to overcome the various challenges, although, a single control cannot address all the issues. Since the different objectives operate in different time scales with varying time constants, a hierarchical control (HC) scheme is considered appropriate for microgrid control [4,6]. Generally, a three-levelled HC scheme is considered with primary, secondary, and tertiary controls. The different control layers operate in a decoupled manner, while exchanging relevant information with each other [6]. The tertiary layer, also know as the EMS, is responsible for the supervising and optimizing the microgrid operation based on predefined objectives. Furthermore, it can communicate with several components in the microgrids and supervise their operation.

Many microgrid control strategies have been described in literature employing a variety of algorithms. Model predictive control (MPC) based methods have been used in [7–9]. MPC is an appealing power

* Corresponding author.
E-mail address: sc421@snu.edu.in (S. Chopra).

https://doi.org/10.1016/j.ijepes.2022.108140
Received 9 September 2021; Received in revised form 21 January 2022; Accepted 18 March 2022
Available online 12 April 2022

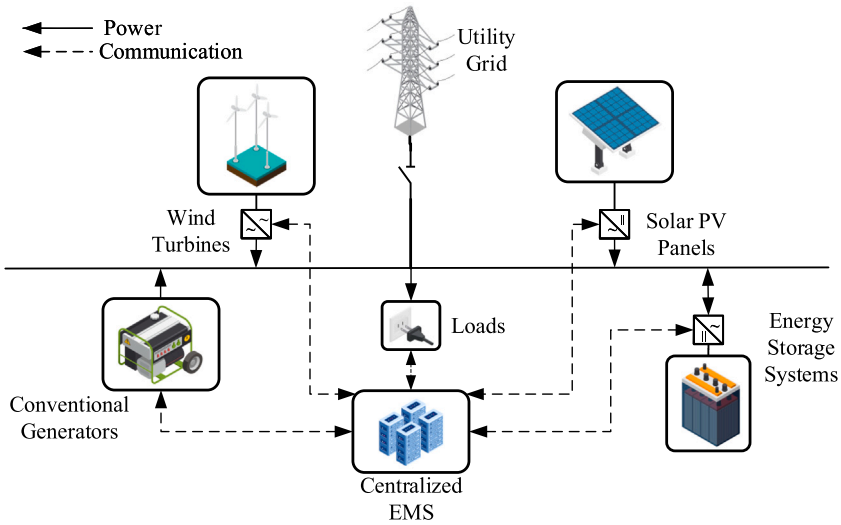

Fig. 1. Microgrid schematic representation.

system control strategy due to its capability to account for predictions in the system behaviour [7]. Heuristic methods, such as particle swarm optimization (PSO), have also been used for optimizing microgrid operation [10,11] and energy management of multiple microgrids [12]. The contributions in [13,14] provide an exhaustive and detailed review of the various types of algorithms and methods used in literature for microgrid energy management, along with the tools used, optimization objectives and constraints.

Droop-based methods have also been used for energy management. In islanded AC microgrids, the DGs are also responsible for maintaining voltage and frequency [15], along with sharing the power to be supplied to the load [2,16], which can be done by using droop-based methods. In [17], the proposed EMS uses a double derivative based droop controller to find a compromise between accurate power sharing among the DGs and microgrid stability using small signal analysis. In [18], an optimal power flow (OPF)-based power sharing EMS for hybrid AC/DC microgrids is proposed to optimize the DG droop characteristics, while also preserving the stable power sharing in the system. The method further regulates the AC/DC voltage and the system frequency. The inclusion of power-flow in the EMS ensures power balance in the system. In [19], the authors describe an extended optimal power flow (EOPF)-based hierarchical scheme for the control of islanded AC microgrids. This work uses a modified power-flow formulation which includes the effect of the primary droop control and aims to find droop coefficients for the DGs while regulating the PCC voltage to 1 p.u. and maximizing the microgrid efficiency. In previous works, the energy management strategies include only the primary droop characteristics in their formulation. However, if secondary control is also included in the power-flow formulation, maintaining bus voltages and system frequencies as optimization objectives or constraints would not be required. Furthermore, the inclusion of both primary and secondary control represent the dynamics of the DG units more accurately [20]. This is the basis of the EMS proposed in this paper.

This paper presents an offline EOPF-based hierarchical scheme for islanded AC microgrids that makes use of a modified power-flow formulation. This formulation includes both primary and secondary control within the power-flow and is modelled as a new type of bus so as to more accurately represent the steady-state dynamics of the system. Additionally, the paper explores the impact of introducing soft limits for bus voltages and considering multiple droop coefficients over the time horizon for the optimization. This can enhance the flexibility of the energy management algorithm and contribute to maintaining a reliable system operation. To validate the proposed energy management algorithm, two case studies are addressed using a modified 14-bus MV CIGRE benchmark microgrid.

The rest of the paper is organized in the following manner. Section 2 describes the different levels of the microgrids HC. Section 3 presents the modified power-flow formulation. In Section 4, the proposed EOPF algorithm is described in detail. Section 5 contains the data for modified CIGRE benchmark microgrid considered in this paper. In Section 6, two different cases are simulated using the proposed EOPF algorithm and the results are analysed. Finally, concluding remarks are given in Section 7.

2. On the microgrid operation management and control

A microgrid can operate in grid-connected or islanded mode. The islanding operation may be due to intentional reasons such as maintenance or security issues, or it may be due to some unintentional reasons such as faults, component failure, etc [2]. In either case, there is a need to control the microgrid with its various DERs to provide proper active and reactive power-sharing among the DGs, and to maintain voltage and frequency within the desirable limits. Since dynamics with different time constants are involved in the system and a single control cannot manage multiple operational targets, a hierarchical control (HC) scheme is required. It consists of three levels: primary, secondary, and tertiary control.

2.1. Primary control

Primary control is the first response to any change in the system condition. It gives the reference points to the voltage and current control loops of DG units, adding virtual inertia in the system and controls their output impedance [21]. This principle can be implemented in Voltage Source Converters by the use of well known P/Q droop method. The power injection for each DG units in the microgrid is given by frequency ω in relation with active power P, and voltage V with reactive power Q given in (1) and (2).

$$\omega = \omega^* - K_n^p \, P_n \tag{1}$$

$$V_n = V_n^* - K_n^q \, Q_n \tag{2}$$

where ω^* is the reference angular frequency of the system, V_n^* is the reference voltage amplitude, and K_n^p and K_n^q are droop coefficients for the nth bus.

2.2. Secondary control

The secondary control regulates the voltage magnitude and frequency to their nominal values for any change of load or generation in

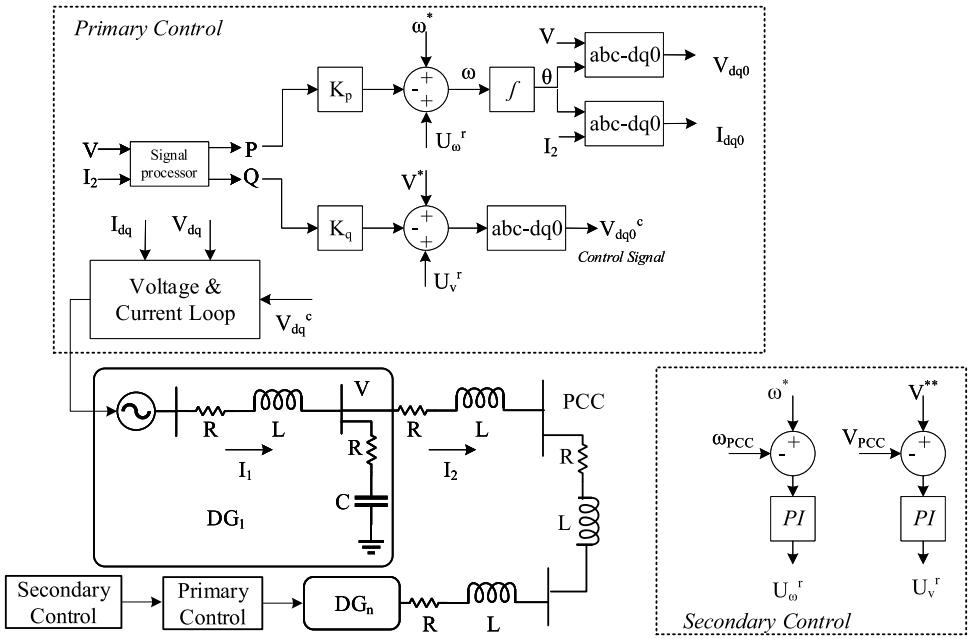

Fig. 2. Hierarchical control with primary and secondary control.

a microgrid. It has a slower time response than the primary control due to some limitations such as availability of primary sources and battery capacity [3]. As shown in Fig. 2, the controlled DG units are connected through RL and RC filters to a PCC bus. The secondary control measures the voltage and frequency at the PCC bus and compares it with the references ω^* and $|V^{**}|$. The error is given to the proportional integral (PI) controller to obtain the output signals U_w^r and U_v^r as given in (3) and (4) [21].

$$U_w^r = K^{pw}(\omega^* - \omega_m) + K^{iw}\int(\omega^* - \omega_m)\,dt \tag{3}$$

$$U_v^r = K^{pv}(|V^{**}| - |V_m|) + K^{iv}\int(|V^{**}| - |V_m|)\,dt \tag{4}$$

where, K^p and K^i are the proportional and integral gains for voltage and frequency, respectively. The output signals U_w^r and U_v^r of PI controllers are sent to the primary control for voltage and frequency restoration. Following this modification, the droop Eqs. (1) and (2) are modified as follows,

$$\omega = \omega^* - K_n^p.P_n + U_w^r \tag{5}$$

$$V_n = V_n^* - K_n^q.Q_n + U_v^r \tag{6}$$

2.3. Tertiary control

The tertiary control incorporates an EMS that accounts for the efficiency and economic concerns in the optimal operation of the microgrid. Although some papers assign EMS to the secondary level and describe tertiary control for multiple microgrid coordination, EMS can also be used at the tertiary level [22].

The EMS is operated in two different modes: centralized and decentralized mode [14,22]. In a centralized mode, the central controller optimizes the exchange of power-flow between the microgrid and the main grid or between microgrids. However, the controller should be sufficiently powerful to process the computational burden and data of the entire system. Moreover, if a fault occurs, it may cause a breakdown of the entire system. Decentralized control addresses these problems, however, it has its own set of drawbacks. It offers more flexibility in operation but requires a sophisticated communication system for proper coordination and synchronization. Thus, depending on the size and operation of the microgrid, a suitable scheme is used [14,22]. However, regardless of the type of control, the main objective of an EMS is to ensure reliable and flexible operation of microgrid.

The EMS operates in the order of minutes. The primary and secondary control have a comparable operation time which is much less than that of an EMS. Hence the EMS's output can be considered as a constant input for lower-level controls that operate in the order of a few seconds or less [2]. An EMS involves various decision making processes to satisfy the required objectives of the system under various constraints [13,14]. Some of these objectives are minimizing green house gas emission, minimizing the operating cost of CGs, minimizing RES curtailment, etc., subject to constraints such as generation limits, ESS storage capacity, bus voltage and frequency among others.

3. Microgrid power-flow

Conventional power-flow techniques cannot be used for islanded microgrids due to following reasons [19]:

(1) The DG units in the microgrid have limited capacity, hence the slack bus cannot be assigned for all the operating conditions.
(2) In an islanded microgrid frequency is continuously varying and cannot be assumed as constant.
(3) The active and reactive power sharing among the DG units, and local bus voltages are not pre-specified and hence, the buses cannot be classified as PQ or PV buses. Moreover, the power sharing among the DG units depends on droop characteristics.

Thus, there is a need for modifying the power-flow formulation to overcome these shortcomings. The modified power-flow formulation employs a new bus type in the conventional Newton–Raphson power flow to maintain its quadratic convergence regardless of microgrid topology, stability, control and presence of non-linear loads [23].

3.0.1. Primary control — Droop Bus

A droop-based control for islanded AC microgrids is integrated with power-flow and optimization in [19]. The method makes use of the well-known droop relations (1) and (2) to calculate the reference or scheduled powers of the buses needed to estimate the power mismatch matrix for Newton–Raphson (NR) power-flow. Moreover, an additional relation is added to take into account the microgrid frequency. The

microgrid frequency is always fluctuating and cannot be assumed to be constant, as in conventional power-flow formulation. Hence, one of the bus phase angles are required to be taken as reference for the other buses [19]. This additional equation is also derived from the active power-droop relation. This formulation further requires fixing the bus angle δ of one of the buses as a reference. The incorporation of primary control leads to the definition of a new type of bus in the microgrid, namely the Droop Bus [19].

3.0.2. Secondary control — HCPQ bus

The Droop Bus formulation, however, only represents the grid-forming primary control in a DG unit. In practical applications, the DG unit would also possess secondary control for voltage amplitude and frequency restoration, i.e., in steady state the assumptions $|V_m| = |V_m^{**}|$ and $\omega = \omega^*$ can be made. To include these functionalities, the secondary control equations are needed, which are described in (5) and (6). The modified equations needed to incorporate secondary control in the formulation for frequency and voltage amplitude restoration are described as follows [20],

$$P_n^{(scheduled)} = \frac{-K^{iw}(\delta_m - \delta_m^0)}{K_n^p} \tag{7}$$

where δ_m^0 is the initial condition and δ_m is the bus voltage angle of the mth bus. All the bus phase angles are automatically computed by the secondary frequency control (7). There is no need to fix a bus as reference as in the case with the Droop Bus formulation.

$$Q_n^{(scheduled)} = \frac{|V_n^*| - |V_n| + U_v^{int}}{K_n^q} \tag{8}$$

where U_v^{int} is the integral part of U_v^r from (4). There is no way to directly calculating U_v^{int}. Nevertheless, since the voltage magnitude of the secondary voltage controlled bus m is already known, as it is fixed to the reference, the reactive power equation for that bus is not needed for estimating the bus voltage magnitude. The reactive power mismatch equation from this secondary voltage controlled bus m is kept in the power mismatch matrix but, instead of finding the bus voltage magnitude, it is used to find the secondary integral term [20].

This leads to the formulation of a new type of bus for microgrids, namely the hierarchically controlled PQ (HCPQ) bus [20]. The power mismatch vector can hence be formulated as follows,

$$\begin{bmatrix} \Delta P_n \\ \Delta Q_n \end{bmatrix} = \begin{bmatrix} P_n^{(scheduled)} - P_n^{(calculated)} \\ Q_n^{(scheduled)} - Q_n^{(calculated)} \end{bmatrix} \tag{9}$$

This formulation includes the effect of both primary and secondary controls and hence, is a more accurate representation of the microgrid dynamics.

4. EOPF based energy management formulation

The combination of the HCPQ bus formulation from Section 3 with a tertiary level optimization layer leads to the proposed EOPF-based energy management algorithm formulation. The inner, power-flow level regulates bus voltages, system frequency, and ensures power balance considering the primary and secondary control steady-state dynamics, while the outer level optimizes the system objectives and ensures that the various system components are operating within their technical limitations. The outer level is also tasked with finding optimal values for certain variables, especially the droop coefficients K_n^p and K_n^q of the HCPQ buses, that are needed for the calculations in the inner level. To better understand the proposed energy management algorithm, a flowchart is illustrated in Fig. 3.

The proposed energy management algorithm works in the following way,

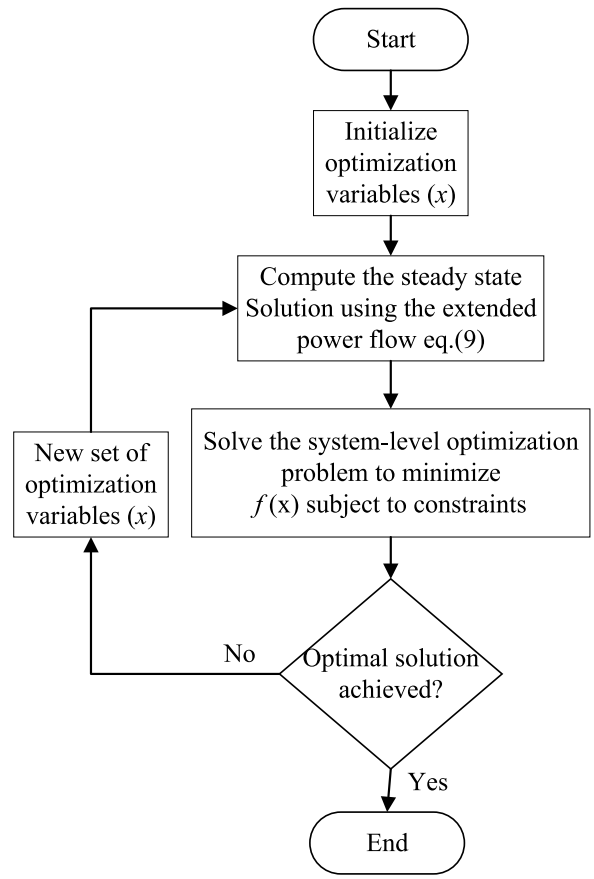

Fig. 3. Proposed EOPF based energy management algorithm flowchart.

(1) Initialize a set of variables to optimize. These variables include the droop coefficients of the HCPQ buses, active and reactive power references of CGs on PQ buses, active power reference for CGs on PV buses, and bus voltages for HCPQ and PV buses. Other variables maybe be included depending on the system components and objectives:
   - In case if BESS is present in the system, the change in the state of charge (SOC) for each time interval.
   - If load shedding is included, the amount of load that can be shed.

(2) For the initialized variables, compute steady-state solution using NR power flow with the HCPQ bus formulation Eqs. (7) and (8).
(3) System-level optimization problem is solved, subject to constraints.
(4) If the solution does not satisfies the constraints and tolerance limits, the entire process is repeated from Step 2 with a new set of variables.
(5) If the solution satisfies the constraints and tolerance limits, the solution is postulated as the optimal solution and the optimization process is ended.

The inclusion of bus voltages for PV and HCPQ buses as optimization variables adds flexibility to the system by not fixing the voltage to an exact, ideal value of 1 p.u. Allowing the voltage to vary within an allowable range implies that the DGs are not forced to maintain their bus voltages by generating, or in certain cases absorbing, a certain amount of reactive power to keep the system in balance throughout the time horizon. Thus, arises the requirement of soft limits for the bus voltages.

Secondly, in case the system has RES, a modification needs to be made. Normally, buses with RES would be HCPQ buses. However, if that particular RES is not giving any power during a time interval, such as buses with SPVs during the night, the maximum possible power output from those buses drops down to zero. The optimization requires the DGs on HCPQ buses to generate within their operational limits. If the maximum and minimum limits are both zero, the power would need to be optimized to exactly zero. However, the droop coefficients would also have their lower and upper boundaries. From (7), we see that for active power to be exactly zero, either the active power droop coefficient K_n^p would need to be infinite, or $\delta_m = \delta_m^0$, which would not be possible if loads are also present on those buses. Similarly, for reactive power in (8) to be zero, either the reactive power droop coefficient K_n^q would need to be infinite, or the numerator would need to be zero, either of which may not be numerically feasible. Hence to overcome this issue, those buses become PQ buses with zero active and reactive power outputs during those time intervals.

Two different cases are considered in this paper,

(1) Minimizing the CG operational cost and RES curtailment.
(2) Minimizing the CG operational cost with the inclusion of load shedding constraints.

and their optimization problems are modelled as described in the following sections.

4.1. Case I: Minimizing the CG operational cost and RES curtailment

Increased penetration of RES into the distribution network reduces the need of CGs to meet the demand, thereby lowering the carbon emissions. Although, when RES penetration exceeds the system's real demand, it produces a slew of concerns, including excessive line losses, transformer and feeder overloading, protection failure, and overvoltage concerns, etc.[24]. As a result, RES curtailment is necessary. This is done by introducing a penalty factor for curtailed RES power C_{RES}. The optimization problem is as follows,

$$f(x) = \min_x \sum_{t=1}^{T_H} \sum_{g=1}^{N_G} (a_g P_g^2(t) + b_g P_g(t) + c_g) + \sum_{t=1}^{T_H} \sum_{N=1}^{N_{RES}} C_{RES} \cdot P_{RES}(t)$$
$$where,\ x = \{K_n^p,\ K_n^q,\ \Delta SOC(t),\ P_{CG}(t),\ Q_{CG}(t),\ V_{PV}(t)\ and\ V_{HCPQ}(t)\} \tag{10}$$

$$subject\ to,\ P_{BESS}(t) + E \cdot \Delta SOC(t) = 0 \tag{11}$$

$$P_{g,\ RES}^{min}(t) \le P_{g,\ RES}(t) \le P_{g,\ RES}^{max}(t) \tag{12}$$

$$Q_{g,\ RES}^{min}(t) \le Q_{g,\ RES}(t) \le Q_{g,\ RES}^{max}(t) \tag{13}$$

$$K_n^{q\ min} \le K_n^q \le K_n^{q\ max} \tag{14}$$

$$K_n^{p\ min} \le K_n^p \le K_n^{p\ max} \tag{15}$$

$$\frac{P_{BESS(d)}(t)}{-E} \le \Delta SOC(t) \le \frac{P_{BESS(c)}(t)}{-E} \tag{16}$$

$$SOC^{min} \le SOC(t) \le SOC^{max} \tag{17}$$

$$V_{PV}(t)^{min} \le V_{PV}(t) \le V_{PV}(t)^{max} \tag{18}$$

$$V_{HCPQ}(t)^{min} \le V_{HCPQ}(t) \le V_{HCPQ}(t)^{max} \tag{19}$$

Where P_{RES} is the curtailed RES power and x is the set of variables to optimize the given objective function, that consists of droop coefficients K_n^p and K_n^q, change in the state of charge of a battery, active P_{CG} and reactive power Q_{CG} contribution from CGs, V_{PV} and V_{HCPQ} voltage soft limits for PV and HCPQ buses. The cost coefficients for the CGs were taken from [8,25].

4.2. Case II: Minimizing the CG operational cost with the inclusion of load shedding constraints

Load shedding is a technique where intentional shutdown of load takes place in parts or part of the distribution system. It is employed to prevent system failure when the actual demand in the system is greater than the available generation.

The optimization objective function (10) is modified as follows for the inclusion of load shedding,

$$f(x) = \min_x \sum_{t=1}^{T_H} \sum_{g=1}^{N_G} (a_g P_g^2(t) + b_g P_g(t) + c_g) + \sum_{t=1}^{T_H} \sum_{l=1}^{N_L} VOLL \cdot P_l(t)$$
$$where,\ x = \{K_n^p,\ K_n^q,\ \Delta SOC(t),\ P_l(t),\ P_{CG}(t),\ Q_{CG}(t),\ V_{PV}(t)\ and\ V_{HCPQ}(t)\} \tag{20}$$

The optimization variables for this case remain the same as those described in case I, with the inclusion of an additional variable P_l for load shed, and the parameter VOLL or value of loss of load. The constraints also remain the same as case I, with the addition of constraints for load shed P_l,

$$0 \le P_l(t) \le P_{LS}^{max}(t) \tag{21}$$

The boundaries for the droop coefficients are assumed as follows for the entire study,

$$2 \times 10^{-7} \le K_n^p \le 5 \times 10^{-4} \tag{22}$$

$$2 \times 10^{-6} \le K_n^p \le 5 \times 10^{-3} \tag{23}$$

5. Modified CIGRE benchmark system

The proposed EOPF energy management algorithm for islanded AC microgrids is tested on a three-phase balanced modified medium voltage (MV) CIGRE benchmark network [8,25,26]. A single-line diagram of 14-bus 12.47 kV test system is shown in Fig. 4. The system consists of DG units with a total installed capacity of 4290 kW and a battery energy storage system (BESS) with capacity of 1000 kWh with its parameters given in Table 5 in Appendix. The different DER capacities are given in Table 6 in Appendix. The typical hourly normalized profiles for wind and solar outputs are shown in Fig. 12 in Appendix.

The aggregated industrial and household loads that are connected to the network are shown in Table 7 in Appendix. The normalized hourly industrial and household load profiles are given in [26] where both of these loads follows the same load pattern, but with different load scaling depending on power consumption by the customers. The total system load capacity for active load is 0.4425 p.u, and 0.0841 p.u. for reactive load as given in Table 7. Since the total DG capacity is 4290 kW, which is much higher than the load, the load would need to be increased by an appropriate factor. The system base is chosen as 1000 kVA. The power factor of 0.8 is considered to calculate the reactive power capacities of the DG units. The detailed information of line parameters connecting the buses in the CIGRE grid are given in Table 8 in the Appendix and the transformer parameters are taken from [8]. According to IEC 60038 [27], the voltage limits are considered as +5% and −10% of nominal value and from EN 50160 [28], the frequency limits of ±1% of nominal frequency are considered for the optimal power flow analysis of the MV modified CIGRE microgrid.

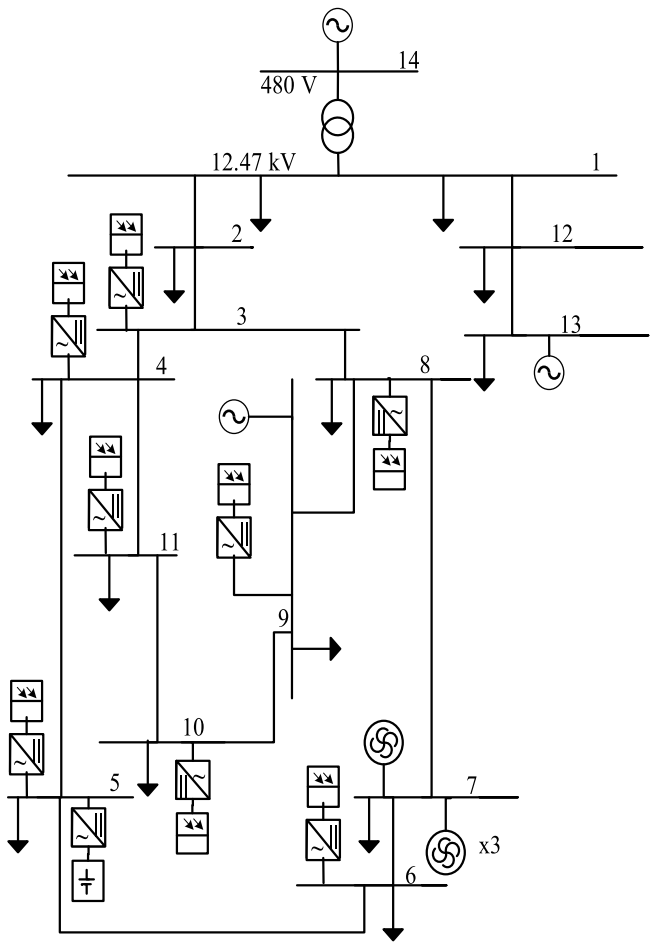

Fig. 4. The modified CIGRE benchmark network under study.

6. EOPF-based energy management assessment

In this section, the proposed energy management algorithm is simulated on the modified CIGRE grid to optimize different cases,

(1) Minimizing the CG operational cost and RES curtailment.
(2) Minimizing the CG operational cost with the inclusion of load shedding constraints.

and to assure the system components are operating well within their constraints and operating limits. The simulations were performed in MATLAB using *fmincon* function with *SQP* algorithm on a computer with processor Intel (R) Core (TM) i5 - 8250U CPU @ 1.60 GHz, 1800 MHz with 8 GB RAM.

6.1. Case I: Minimizing the CG operational cost and RES curtailment

The penalty factor for curtailed RES power C_{RES} is assumed as 50$/MW throughout this study. The load was increased by a factor of 3. To evaluate the system behaviour for cost minimization of CGs and RES curtailment, ±1% voltage soft limits for PV and HCPQ buses are considered and all the loads were linear. These voltage variables from the optimization level are used as a reference for respective buses in hierarchically controlled power-flow formulation. The simulation took 36 iterations and the cost was optimized to $ 682,575.29. Fig. 5 shows the active power balance and hourly utilized RES active power for 1% voltage soft limits. It is observed that, there is no contribution from CGs for active power balance, which is in line with the optimization objectives of minimizing CG operational cost and RES curtailment. The total RES active power utilized is 55.98%. BESS on the other hand, supports the optimization objective by managing the excess RES active power, which can be seen from Fig. 5. The SOC and battery charging and discharging power are shown in Fig. 6.

Moreover, the system behaviour is also analysed in the presence of non-linear loads. The linear loads connected to bus 3 and 12 are replaced by voltage-dependent non-linear loads. The expression for non-linear loads is given in [29]. The presence of voltage-dependent non-linear loads increases the optimization cost by 0.227% and the simulation optimized to a cost of $ 684,126.74 after 13 iterations. From Fig. 7, it is observed that the voltage on HCPQ bus 3 is optimized to more than 1 p.u. over the entire time horizon T_H and therefore the load increases by 0.141 kW on this bus, compared to the case with linear loads and ±1% voltage soft limits. On the other hand, bus 12 is a PQ bus with one of the largest connected load, and the voltage stays below 1 p.u. for majority of the time horizon. Hence, the total system load is reduced by 28.368 kW increasing the RES curtailment and overall cost in the system. This also reduces the RES power utilized in the system by 0.10%.

The optimized droop coefficients with 1% voltage soft limits and linear loads, and in the presence of non-linear loads are given in Table 1.

From Table 2, it is observed that the cost increases with a decrease in RES power utilization due to the reduction of total load in the presence of voltage-dependent non-linear loads. However, due to this decrease in RES power utilization, the losses in the system are also reduced.

6.2. Case II: Minimizing the CG operational cost with the inclusion of load shedding constraints

To analyse the load shedding scenario in the system, a load profile with larger load values has been considered in this case. Consequently, the load is increased by a factor of 7. The load on bus 12 is used for load shedding, which is a PQ bus and hosts one of the largest loads in the system. The maximum load that can be shed is assumed to be 20% of the total demand at that particular hour.

On simulating the cost minimization objective with load shedding constraints in MATLAB with ±1% voltage soft limits and 0.1 $\$/kW$ VOLL, the following results are obtained. The simulation optimized to a cost of $ 4826.90 after 12 iterations. In Fig. 8, it can be seen that all of the permissible load is shed during most of the time horizon. Load shedding minimizes the cost by decreasing the CG contribution. In the hours where there is no load shedding, all the active power is provided by RES, which can be seen from active power balance in Fig. 9. Hence, cutting down on load during these hours would only increase the cost.

The total RES utilization is 83.76%. From the active power balance and the RES utilization results shown in Fig. 9, it is evident that by decreasing the CGs contribution in many hours during the time horizon, the total cost could have been reduced which would have also resulted in reducing their environmental impacts. This does not occur, however, because the droop coefficients for a given bus are fixed over the entire time horizon. When a certain RES is required to provide a large amount of power in a single hour to balance the load, the active power droop coefficient K_n^p for that bus must be less, most likely close to the minimal value. This droop coefficient gets fixed for the entire time horizon, resulting in that particular RES contributing more in other hours as well. As a result, the other RES are forced to deliver less power, and their droop coefficient values may be higher which causes under-utilization of RES.

The BESS action is shown in Fig. 10. During the hour $t = 24$, the BESS SOC does not increase even though there is an excess amount of RES available. This is due to the fact the RES curtailment is not included in the objective function and hence, there is no provision to use the excess RES during that hour. A final constraint can be added to the

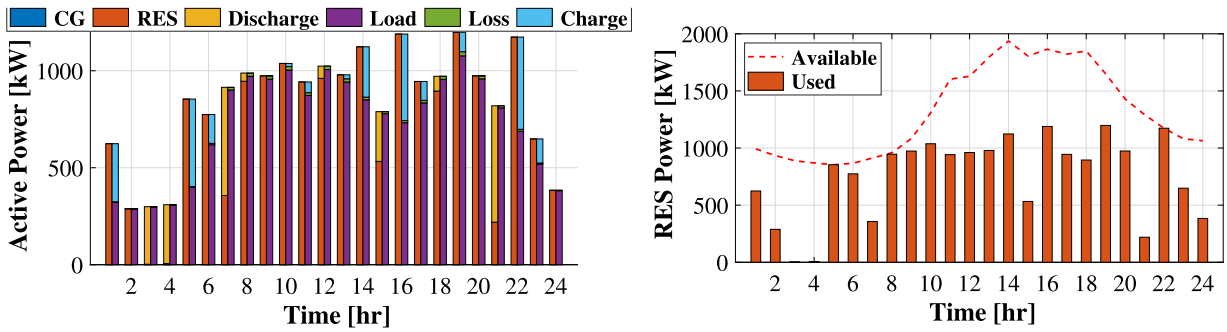

(a) Active Power (b) RES Utilization

Fig. 5. Active power balance and RES utilization for case I with linear loads.

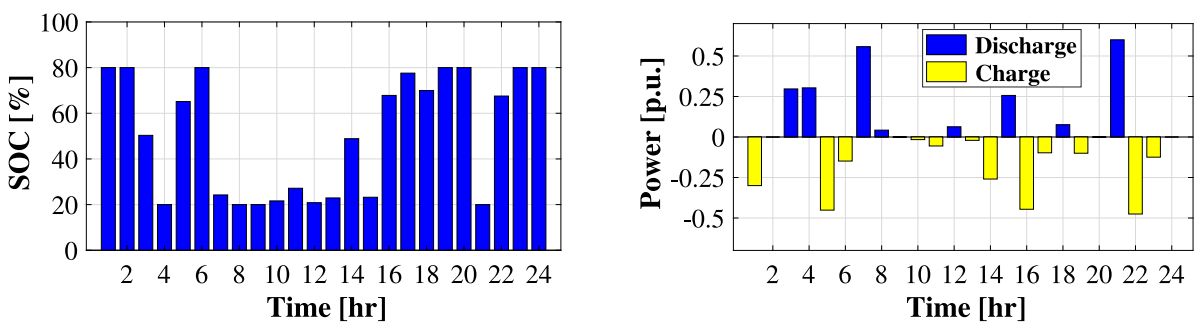

(a) SOC (b) BESS Power

Fig. 6. BESS usage with linear loads.

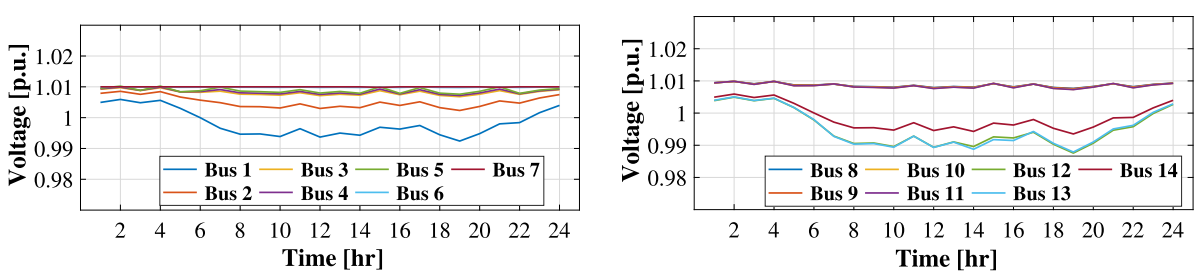

(a) Bus 1-7 (b) Bus 8-14

Fig. 7. Bus voltage magnitudes with inclusion of non-linear loads.

Table 1
Optimized droop coefficients for case I.

	Linear loads		Non-linear loads			Linear loads		Non-linear loads	
Bus	K_n^p	K_n^q	K_n^p	K_n^q	Bus	K_n^p	K_n^q	K_n^p	K_n^q
3	5.0000e−4	4.7478e−3	5.0000e−4	1.3065e−3	7b	5.1390e−7	1.2575e−3	2.0000e−7	2.0000e−6
4	5.0000e−4	3.7590e−3	5.0000e−4	5.0000e−3	8	4.6955e−4	7.0855e−6	5.0000e−4	2.0282e−3
5	4.3363e−4	1.9282e−3	5.0000e−4	5.0000e−3	9	4.7967e−4	1.3897e−3	5.0000e−4	5.0000e−3
6	3.3780e−5	1.5017e−3	3.6543e−5	2.0000e−6	10	5.0000e−4	4.9975e−3	5.0000e−4	2.0000e−6
7a	5.0622e−7	1.2593e−3	2.0000e−7	3.7302e−6	11	5.0000e−4	5.0000e−3	5.0000e−4	3.5968e−3

Table 2
Summary of results for case I.

Scenario	Iterations	Cost [$]	System loss		RES active power used [%]
			[kW]	kVAR	
Linear loads	36	682,575.29	259.22	176.19	55.98
Non-linear loads	13	684,126.74	256.56	174.17	55.88

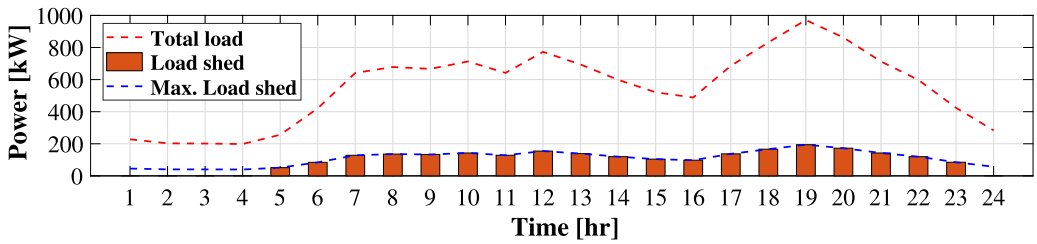

Fig. 8. Load shedding for case II.

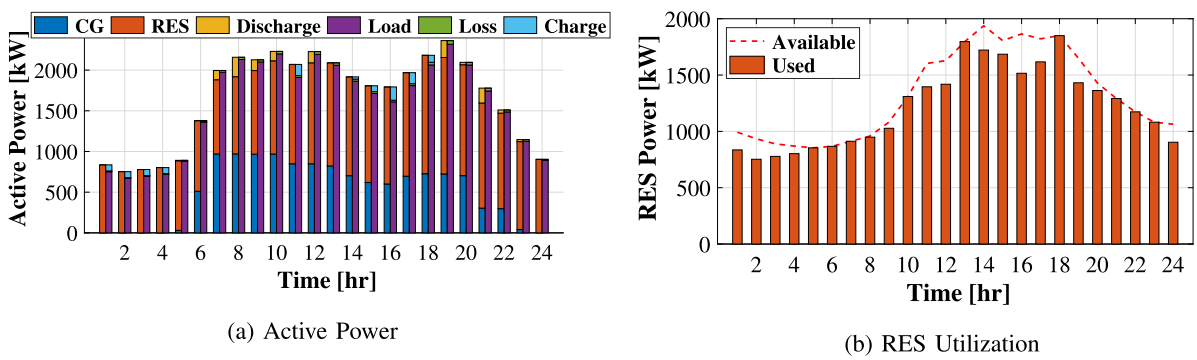

(a) Active Power

(b) RES Utilization

Fig. 9. Active power balance and RES utilization for case II.

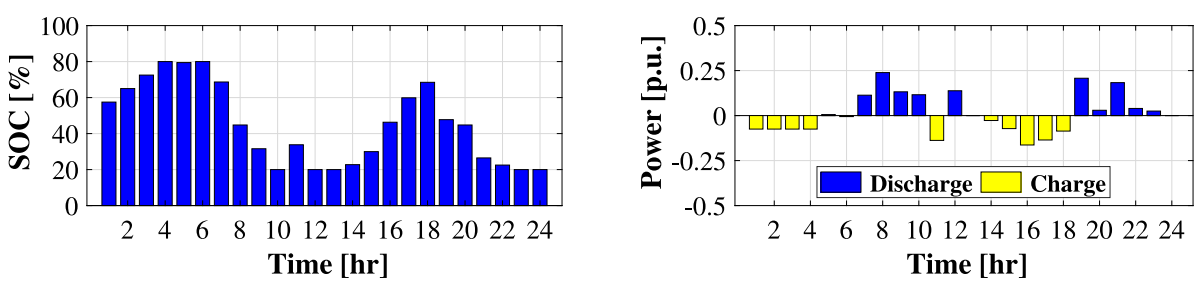

(a) SOC

(b) BESS Power

Fig. 10. BESS usage for case II.

Table 3
Optimized droop coefficients for case II.

Bus	3	4	5	6	7a	7b	8	9	10	11
K_n^p	1.1028e−4	1.1028e−4	7.3555e−5	7.3555e−5	1.6311e−4	2.0268e−7	7.3555e−5	7.3555e−5	5.5137e−4	2.0268e−4
K_n^q	1.6894e−3	3.8220e−4	3.7382e−4	1.4536e−3	4.9603e−6	4.5265e−6	3.3787e−3	5.0000e−3	6.1575e−4	3.0822e−3

above optimization problem in a straight forward manner to ensure a specific amount of SOC at the end of the simulation time.

The optimized variables for fixed droop coefficients for the entire time horizon are given in Table 3. The active power droop coefficient for the 7b, i.e., the 150 kW WTs on bus 7, approaches its minimum limit of 2×10^{-7}, causing the other buses to have a larger droop coefficient. It is also worth noting that on bus 7, the network has three identical 150 kW WTs.

To overcome this drawback of the algorithm, multiple active power droop time frames could be defined for a given bus, each with a set of droop coefficients independent of the other time frames. This way, the 24 hour time frame is divided into 8 smaller time frames of 3 hour duration each for the active power droop coefficient K_n^p. With these modifications, the simulation results show a cost of \$ 3726.29, a reduction of 22.80% as compared to the case with a fixed droop time frame. However, it took 111 iterations to find the results. The load shedding pattern is the same as the 24 hour fixed-droop time frame. This shows that the total amount of power shed remains the same irrespective of the change in the droop time frame. Therefore, the decrease in cost is solely due to a reduction in CGs contribution and an increase in RES active power utilization to 93.57%. which is shown in Fig. 11.

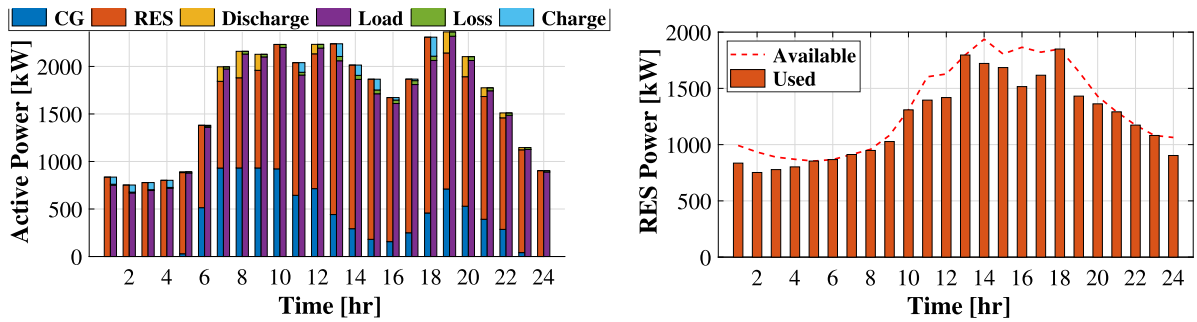

(a) Active Power (b) RES Utilization

Fig. 11. Active power balance and RES utilization for case II with 3 hour droop time frame.

Table 4
Summary of results for case II.

Droop time frame [h]	Cost [$]	Iterations	RES usage [%]	System loss	
				[kW]	[kVAR]
–	4826.90	12	83.76	549.95	476.27
3	3726.29	111	93.57	666.63	544.70

Table 4 illustrates the results obtained for cost minimization of CGs with load shedding for fixed and 3 hour droop time frame. It is seen that for the 3 hour droop time frame the active power contribution from RES is more than the fixed droop time frame case and hence the overall cost reduces. However, this increases the system losses for a 3 hour droop time frame.

From the results of these two case studies, it can be said that the performance of the proposed control scheme is deemed good. The addition of features such as voltage soft limits and varying droop time frames allows for more flexibility in the system. Since the proposed scheme is only for offline use, the computational complexity may be overlooked and it can be used for steady-state modelling and simulation of islanded AC microgrids. The online application of the proposed energy management scheme can be implemented using an interface software called LABVIEW [30] to analyse various operating conditions such as random load and capacity profiles, with the inclusion of practical devices like Smart Meter (SM) for measuring variable loads and to examine the computational time for execution [19]. This methodology has been used in [19], however, the method may or may not apply to the scheme proposed in this paper. Further developments are needed to be analysed for online application of the proposed energy management scheme.

7. Conclusion

This paper proposes a novel EOPF-based hierarchical scheme for islanded AC microgrids. The proposed centralized offline energy management scheme uses the HCPQ bus formulation which takes into account the effect of primary and secondary control dynamics. The energy management algorithm is validated on a modified MV CIGRE benchmark network by performing two different case studies. The simulation results from the case studies indicate a good performance for the proposed energy management algorithm. The optimization objective of minimizing cost was achieved, along with maintaining bus voltages and system frequency within the desired range, securing power balance, and ensuring that the various components are within their operational limits. Additionally, shorter droop time frames and voltage soft limits allow for more flexibility in the system by ensuring reliable operation. In order to judge whether the chosen droop coefficient ranges would ensure a stable system operation, a stability analysis would be required, which was out of the scope in this study. Future works may include extending the control scheme for multi-microgrid system energy management.

Table 5
BESS parameters [8,25].

Parameter	Value	Unit
SOC_0	0.5	–
SOC^{min}	0.2	–
SOC^{max}	0.8	–
P_d^{min}	0	kW
P_d^{max}	900	kW
P_c^{min}	0	kW
P_c^{max}	900	kW
η_d	100	%
η_c	100	%
E	1000	kWh

CRediT authorship contribution statement

Sarthak Chopra: Conceptualization, Methodology, Software, Validation, Writing – original draft. **Gowtham Meda Vanaprasad:** Conceptualization, Methodology, Software, Validation, Writing – original draft. **Gibran David Agundis Tinajero:** Conceptualization, Methodology, Software, Validation, Writing – review & editing. **Najmeh Bazmohammadi:** Conceptualization, Methodology, Software, Validation, Writing – review & editing. **Juan C. Vasquez:** Writing – review & editing, Resources, Funding acquisition. **Josep M. Guerrero:** Writing – review & editing, Resources, Funding acquisition.

Declaration of competing interest

The authors declare that they have no known competing financial interests or personal relationships that could have appeared to influence the work reported in this paper.

Acknowledgement

This work was supported by VILLUM FONDEN, Denmark under the VILLUM Investigator Grant (no. 25920): Center for Research on Microgrids (CROM).

Appendix

See Fig. 12 and Tables 5–8.

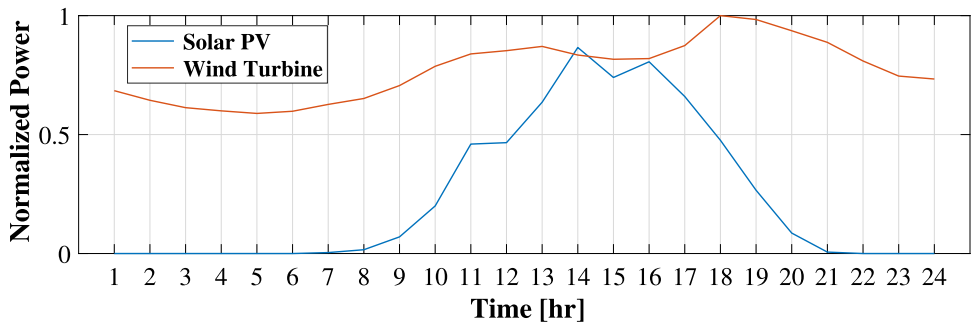

Fig. 12. Normalized wind [31] and PV profiles [32].

Table 6
DER capacity [8,25].

Bus no.	Type	P_{max} [kW]	Bus	Type	P_{max} [kW]
3	SPV	80	7	Wind	150
4	SPV	80	8	SPV	120
5	SPV	120	9	SPV	120
5	BESS	900	9	CG	300
6	SPV	120	10	SPV	160
7	Wind	1000	11	SPV	40
7	Wind	150	13	CG	300
7	Wind	150	14	CG	1400

Table 7
Load parameters at each bus [26].

Bus no.	Load type	P_{max} [p.u.]	Q_{max} [p.u.]	Power factor
1	Household	0.15	0.031	0.980
1	Industrial	0.05	0.01	0.980
2	Household	0.00276	0.00069	0.970
3	Industrial	0.00224	0.00139	0.849
4	Household	0.00432	0.00108	0.970
5	Household	0.00725	0.00182	0.969
6	Household	0.0055	0.00138	0.969
7	Industrial	0.00077	0.00048	0.848
8	Household	0.00588	0.00147	0.970
9	Industrial	0.00574	0.00356	0.849
10	Household	0.00477	0.0012	0.969
11	Household	0.00331	0.00083	0.969
12	Household	0.15	0.03	0.980
13	Industrial	0.05	0.0002	0.999

Table 8
Line parameters [8,26].

From bus	To bus	Length [km]	R [Ω/km]	X [Ω/km]
1	2	2.8	0.579	0.367
2	3	4.4	0.164	0.113
3	4	0.6	0.262	0.121
4	5	0.6	0.354	0.129
5	6	1.5	0.336	0.126
6	7	0.2	0.256	0.13
7	8	1.7	0.294	0.123
8	9	0.3	0.339	0.13
9	10	0.8	0.399	0.133
10	11	0.3	0.367	0.133
11	4	0.5	0.423	0.134
3	8	1.3	0.172	0.115
12	13	3	0.337	0.358
1	12	4.9	0.337	0.358

References

[1] Zhao B, Wang X, Lin D, Calvin MM, Morgan JC, Qin R, et al. Energy management of multiple microgrids based on a system of systems architecture. IEEE Trans Power Syst 2018;33(6):6410–21.

[2] Olivares DE, Mehrizi-Sani A, Etemadi AH, Cañizares CA, Iravani R, Kazerani M, et al. Trends in microgrid control. IEEE Trans Smart Grid 2014;5(4):1905–19. http://dx.doi.org/10.1109/TSG.2013.2295514.

[3] Palizban O, Kauhaniemi K, Guerrero JM. Microgrids in active network management—Part I: Hierarchical control, energy storage, virtual power plants, and market participation. Renew Sustain Energy Rev 2014;36:428–39.

[4] Meng L, Luna A, Díaz ER, Sun B, Dragicevic T, Savaghebi M, et al. Flexible system integration and advanced hierarchical control architectures in the microgrid research laboratory of Aalborg university. IEEE Trans Ind Appl 2015;52(2):1736–49.

[5] Rajesh KS, Dash SS, Rajagopal R, Sridhar R. A review on control of ac microgrid. Renew Sustain Energy Rev 2017;71:814–9.

[6] Meng L, Savaghebi M, Andrade F, Vasquez JC, Guerrero JM, Graells M. Microgrid central controller development and hierarchical control implementation in the intelligent microgrid lab of Aalborg university. In: 2015 IEEE applied power electronics conference and exposition. IEEE; 2015, p. 2585–92.

[7] Bazmohammadi N, Tahsiri A, Anvari-Moghaddam A, Guerrero JM. Stochastic predictive control of multi-microgrid systems. IEEE Trans Ind Appl 2019;55(5):5311–9.

[8] Olivares DE, Canizares CA, Kazerani M. A centralized energy management system for isolated microgrids. IEEE Trans Smart Grid 2014;5(4):1864–75.

[9] Bazmohammadi N, Tahsiri A, Anvari-Moghaddam A, Guerrero JM. Optimal operation management of a regional network of microgrids based on chance-constrained model predictive control. IET Gener Transm Distrib 2018;12(15):3772–9.

[10] Aghajani GR, Shayanfar HA, Shayeghi H. Presenting a multi-objective generation scheduling model for pricing demand response rate in micro-grid energy management. Energy Convers Manage 2015;106:308–21.

[11] Aghajani GR, Shayanfar HA, Shayeghi H. Demand side management in a smart micro-grid in the presence of renewable generation and demand response. Energy 2017;126:622–37.

[12] Bazmohammadi N, Karimpour A, Bazmohammadi S, Anvari-Moghaddam A, Guerrero JM. An efficient decision-making approach for optimal energy management of microgrids. In: 2019 IEEE Milan PowerTech. IEEE; 2019, p. 1–6.

[13] Ahmad Khan A, Naeem M, Iqbal M, Qaisar S, Anpalagan A. A compendium of optimization objectives, constraints, tools and algorithms for energy management in microgrids. Renew Sustain Energy Rev 2016;58:1664–83.

[14] Shayeghi H, Shahryari E, Moradzadeh M, Siano P. A survey on microgrid energy management considering flexible energy sources. Energies 2019;12(11):2156.

[15] Vandoorn TL, Vasquez JC, De Kooning J, Guerrero JM, Vandevelde L. Microgrids: Hierarchical control and an overview of the control and reserve management strategies. IEEE Trans Ind Electron Mag 2013;7(4):42–55.

[16] Chowdhury S, Crossley P. Microgrids and active distribution networks. IET renewable energy series, Institution of Engineering and Technology; 2009.

[17] Firdaus A, Mishra S. A double derivative based droop controller for improved power sharing in inverter based autonomous microgrid. In: 2018 IEEMA engineer infinite conference. IEEE; 2018, p. 1–6.

[18] Eajal AA, Yazdavar AH, El-Saadany EF, Salama MM. Optimizing the droop characteristics of AC/DC hybrid microgrids for precise power sharing. IEEE Syst J 2020.

[19] Agundis-Tinajero G, Aldana NLD, Luna AC, Segundo-Ramirez J, Visairo-Cruz N, Guerrero JM, et al. Extended-optimal-power-flow-based hierarchical control for islanded AC microgrids. IEEE Trans Power Electron 2018;34(1):840–8.

[20] Agundis-Tinajero G, Segundo-Ramírez J, Visairo-Cruz N, Savaghebi M, Guerrero JM, Barocio E. Power flow modeling of islanded AC microgrids with hierarchical control. Int J Electr Power Energy Syst 2019;105:28–36.

[21] Guerrero JM, Vasquez JC, Matas J, de Vicuna LG, Castilla M. Hierarchical control of droop-controlled AC and DC microgrids: A general approach toward standardization. IEEE Trans Ind Electron 2011;58(1):158–72.

[22] Meng L, Sanseverino ER, Luna A, Dragicevic T, Vasquez JC, Guerrero JM. Microgrid supervisory controllers and energy management systems: A literature review. Renew Sustain Energy Rev 2016;60:1263–73.

[23] Agundis-Tinajero G, Segundo-Ramírez J, Visairo-Cruz N, Savaghebi M, Guerrero JM, Barocio E. Power flow modeling of islanded AC microgrids with hierarchical control. Int J Electr Power Energy Syst 2019;105:28–36. http://dx.doi.org/10.1016/j.ijepes.2018.08.002.

[24] Ismael SM, Aleem SHA, Abdelaziz AY, Zobaa AF. State-of-the-art of hosting capacity in modern power systems with distributed generation. Renew Energy 2019;130:1002–20.
[25] Bazmohammadi N, Tahsiri A, Anvari-Moghaddam A, Guerrero JM. A hierarchical energy management strategy for interconnected microgrids considering uncertainty. Int J Electr Power Energy Syst 2019;109:597–608.
[26] Rudion K, Orths A, Styczynski ZA, Strunz K. Design of benchmark of medium voltage distribution network for investigation of DG integration. In: 2006 IEEE power engineering society general meeting. 2006.
[27] Voltages, IEC Standard. IEC 60038, vol. 7. 2009.
[28] Markiewicz H, Klajn A. Voltage Disturbances Standard EN 50160 - Voltage Characteristics in Public Distribution Systems. Copper Development Association; 2008.
[29] Vural AM. Interior point-based slack-bus free-power flow solution for balanced islanded microgrids. Int Trans Electr Energy Syst 2016;26(5):968–92.
[30] Elliott C, Vijayakumar V, Zink W, Hansen R. National instruments LabVIEW: A programming environment for laboratory automation and measurement. JALA 2007;12(1):17–24.
[31] Soroudi A. Power system optimization modeling in GAMS, vol. 78. Springer; 2017.
[32] Tsikalakis AG, Hatziargyriou ND. Centralized control for optimizing microgrids operation. In: 2011 IEEE power and energy society general meeting. IEEE; 2011, p. 1–8.